P. V. Denisenko

University of Warwick, Coventry, UK

K. N. Volkov

Kingston University, London, UK

P. S. Chernyshov

BSTU "VOENMEH" named after D.F. Ustinov, St. Petersburg

L. O. Vokin

BSTU "VOENMEKH" named after D.F. Ustinov, St. Petersburg

Numerical simulation of the flow around the impeller of a quadcopter and determination of its thrust characteristics in various flight modes

Numerical modeling is becoming a powerful tool for choosing the aerodynamic configurations of new aircraft and their engines, as well as determining the optimal modes of their operation. To simulate the flow induced by the rotation of the rotor blades of the quadcopter, the full Navier – Stokes equations are used, which describe the flow of a viscous compressible gas. Based on the results of numerical simulation, the characteristics of the impeller are determined in various flight modes, including hovering and oblique airflow at a variable angle of deviation from the vertical.

Key words: quadrocopter, impeller, numerical modeling, aerodynamics, thrust.

Introduction

To ensure the effective functioning of a UAV (Unmanned Aerial Vehicle) in various flight modes at the design stage, it is necessary to solve a number of problems associated with improving the aerodynamic characteristics of the aircraft and its various components. In particular, it is important to determine the characteristics of the propeller and its effect on other parts of the UAV [1]. The available results of numerical and experimental studies show that the operation of the propeller propeller has a significant effect on the aerodynamic forces and moment characteristics of the aircraft [2, 3].

Among the potential small-sized transport aircraft, a new class of relatively small multi-rotor aircraft (rotorcraft) has developed. Quadrocopters (aircraft with four rotor propellers, two pairs of which rotate in opposite directions) have a number of advantages (compactness, maneuverability, low takeoff weight with a significant payload) over other aircraft [4].

Numerical modeling based on modern approaches to the mathematical description of stationary and non-stationary flows of a viscous incompressible fluid is one of the tools for optimizing existing and searching for new schemes and layouts of UAVs. This approach allows both to reduce costs at the preliminary design stage and makes it possible to search for new forms. In this case, it is possible not only to calculate the thrust characteristics, but also to investigate the flow that forms behind the propeller. Improvement of aerodynamic characteristics allows to increase the speed and range of flight, as well as to reduce fuel consumption, increase the stability and controllability of the aircraft.

A method for determining nonlinear aerodynamic characteristics in a non-stationary formulation based on a thin bearing surface is developed in [5]. The possibilities for modeling the aerodynamics of propellers, which are opening up with the advent of the nonlinear unsteady vortex theory of a propeller based on a thin bearing surface, made it possible to start studying the aeroacoustic characteristics of propellers in the far field. The results of experimental studies of the aerodynamic characteristics of a model of a disk-shaped remotely piloted aircraft with a ducted fan under conditions of oblique blowing are given in [6].

Propellers of this type are investigated both by experimental [7–10] and by numerical methods, including the RANS / URANS solution [11–14] and eddy-resolving approaches to the simulation of turbulent flows [15]. A review of experimental and numerical studies is given in [16].

Eddy-resolving methods for modeling turbulent flows (DES) are used in [17] to solve the joint problem of calculating the aeroelastic deformation of propeller blades. Improving the aerodynamic and aeroacoustic characteristics of a quadrocopter is associated with the determination of the optimal parameters of the

impeller. The complexity of calculating the aerodynamic characteristics of impeller at different flight modes is due to the operating conditions of the propeller in the profiled channel and the conditions of the external picture of the incident flow around the body [18–22].

In this work, on the basis of the developed numerical simulation tools, the aerodynamic and thrust characteristics of the impeller are estimated in a wide range of determining parameters. For the calculations, the complete Navier – Stokes equations were set in a rotating coordinate system and modern approaches to modeling turbulent flows are used.

Geometrical model

For the design of the propeller, highly loaded propellers K184V are considered using an air ring, which is a body of revolution with an aerodynamic profile in cross section. The use of an air ring in conditions of a small propeller step (low speed of the flow approaching the propeller) can significantly increase the air flow passing through the rotor rotation loop, increase thrust by creating air circulation around the airfoil of the ring and reduce the power on the propeller. The flow pattern around the impeller largely depends on its geometric parameters. The parameters of the geometric model of this impeller are set based on the analysis of open sources. The propeller diameter is 760 mm, and the diameter of the outlet section of the ring is D mm.

The impeller is shown in Fig. 1. The x-axis of the Cartesian coordinate system coincides with the direction of the incoming flow velocity. The parameter of the model is the angle of deviation of the impeller from the vertical γ.

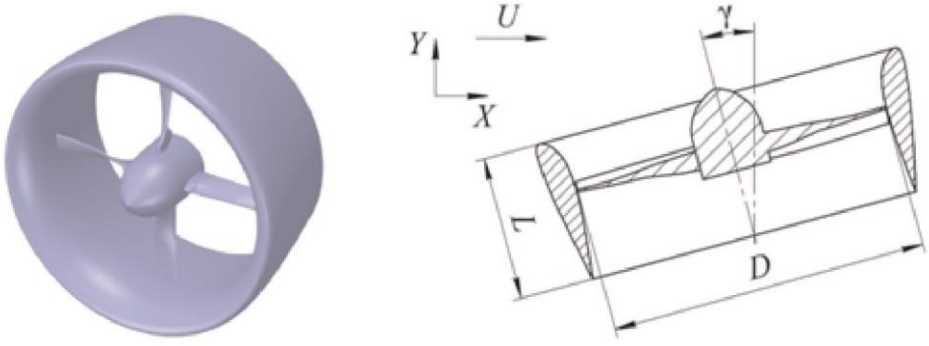

а) б)

Figure 1. Model of a four-bladed IMPELLER with a hub cock (a) and its geometric characteristics (b)

The blade setting angle, which is determined by the angle of rotation of the blade profile, located at a relative radius of 0.75 (where, when setting the blade twist of the airfoil chord, is coplanar to the plane of rotation of the propeller), was calculated for each operating mode separately.

Mathematical model and boundary conditions

To simulate the flow induced by the rotation of the rotor blades of the quadcopter, the full Navier – Stokes equations are used, which describe the flow of a viscous compressible gas. Calculations are carried out to find stationary or non-stationary fields of physical variables that characterize the flow near the impeller and allow determining the aerodynamic loads on the rotor blades and its thrust characteristics.

Turbulent flows are simulated using unsteady Reynolds-averaged Navier – Stokes equations using the SST turbulence model and modeling large eddies using the WALE subgrid viscosity model. The working fluid is air. The density of the fluid changes according to the ideal gas model. The viscosity of the fluid is considered constant.

At the inlet to the computational domain, the velocity and stagnation temperature are set, and the static pressure is fixed at the other boundaries. The degree of turbulence at the inlet boundary is 5%, and the ratio of turbulent viscosity to dynamic viscosity of air is 10. On the walls, adhesion and no-flow conditions are applied for the components, and for temperature, the condition of zero heat flux.

The calculations are carried out on an unstructured mesh consisting of tetrahedral cells. The total number of cells is approximately 3 million. The maximum characteristic cell size in the main part of the region is 0.1 m. Part of the grid with prismatic cells adjoins the solid walls. The thickness of the prismatic layer is assumed to be 1 mm, the number of layers is 5, and the cell growth factor is 1.2.

The geometric model of the impeller is a flow path with built-in rotating parts. The computational domain consists of rotating (rotor) and stationary (stator)

subareas. The sliding grid technology is used to account for their interaction. The rotor and the surrounding elements of the device, which are surfaces of revolution, are calculated in a rotating coordinate system, and the rest - in a stationary coordinate system. The partition boundary is not a structural element of the device, but is an auxiliary surface of revolution that divides the computational grid into several parts. With this approach to solving the problem, the change in the computational grid when the position of the rotating body changes does not occur, since the grid in the rotor rotates behind the moving parts of the device.

To accelerate convergence, a nonzero initial distribution of velocities and pressure is specified. To find them, the frozen rotor model is used, which allows one to obtain a close to real initial distribution of the sought functions on a rather coarse grid. Within the frozen rotor approximation, the geometry freezes in a certain position, which makes it possible to study the flow field for the selected rotor position (the blades are stationary relative to the channel, and centrifugal forces are applied to the surrounding area). When using the frozen rotor model, the updating of the position of the rotating mesh relative to the stationary one is also disabled, which reduces the computation time for one iteration.

Numerical method

The basic equations are discretized using the finite volume method on unstructured grids and the median control volume [23]. The time integration is carried out by the third-order Runge-Kutta method. Discretization of inviscid flows is carried out using the MUSCL scheme (Monotonic Upstream Schemes for Conservation Laws, monotonic upstream scheme for conservation laws), and viscous flows by a centered scheme of the 2nd order of accuracy. Using the MUSCL scheme allows increasing the order of approximation in spatial variables without losing the monotonicity of the solution, satisfying the TVD (Total Variation Diminishing) condition, and applying a combination of second-order centered finite differences and a dissipative term. Switching between them is carried out by limiting the flow based on characteristic variables. Finding the gradient and pseudo-Laplacian at the midpoint of the control volume face is based on ratios adapted for

calculations on highly stretched meshes used in the boundary layer. To solve the system of difference equations, the geometric multigrid method is used [24]. A system of grids of various resolutions is constructed using the Edge-Collapsing Method.

The results of numerical modeling are the pressure and velocity fields both in the design zone and directly on the blade surface, which makes it possible to determine the aerodynamic characteristics of the propeller in various modes.

Based on the results of the numerical calculation, the thrust force created by the propeller blades P_1, the thrust force created due to the circulation around the profile of the impeller ring P_2, the drag force of the propeller hub fairing P_3, and the moment of resistance to rotation M are determined. The resulting power characteristics allow determining the total thrust force of this given conditions $P=P_1+P_2-P_3$. The thrust factor is calculated using the formula $\alpha=P/\rho n^2D^4$, and the power factor is calculated using the formula $\beta=N/\rho n^3D^5$, where ρ is the air density, D is the propeller diameter, P is the thrust force. The required shaft power is determined by the formula $N=\pi nM/30$ [W], where n is the rotation speed [rpm], M is the torque of resistance to rotation [N · m].

Results

The calculation of the gas flow around the impeller with the optimal angles of the propeller blades relative to the incoming flow velocity is performed. The freestream velocity varies from 25 to 75 m/s. For each value of the incoming flow velocity, the optimal angle of rotation of the rotor blade was calculated (60.64 ° at U = 25 m/s, 74.29 ° at U = 50 m/s, 79.38 ° at U = 75 m/s). The impeller tilt angle is 15, 30 and 45 degrees. Ring length L = 337 mm.

The streamlines at different velocities of the incident flow and the angle of deviation of the impeller from the vertical are shown in Fig. 2. In the flow in front of the rotor, the streamlines are directed along the axis of rotation inside the ring, as a result of which the effect of ambient air sucking into the channel formed by the ring is formed. In this case, the value of the velocity decreases along the radius of the ring and becomes negligible on the outer surface. Behind the rotor, there is a

significant acceleration of the axial flow velocity on the cylindrical surface of the order of the radius of the ring and its twisting, co-directional with the direction of rotation of the rotor. As the radius decreases and the distance increases, the axial velocity decreases, and the flow swirl increases. Behind the central body, where the axial velocity is practically zero, the streamlines are twisted into a bundle. In the lower part of the flow in the vicinity of the axis of rotation, spiral vortices are formed.

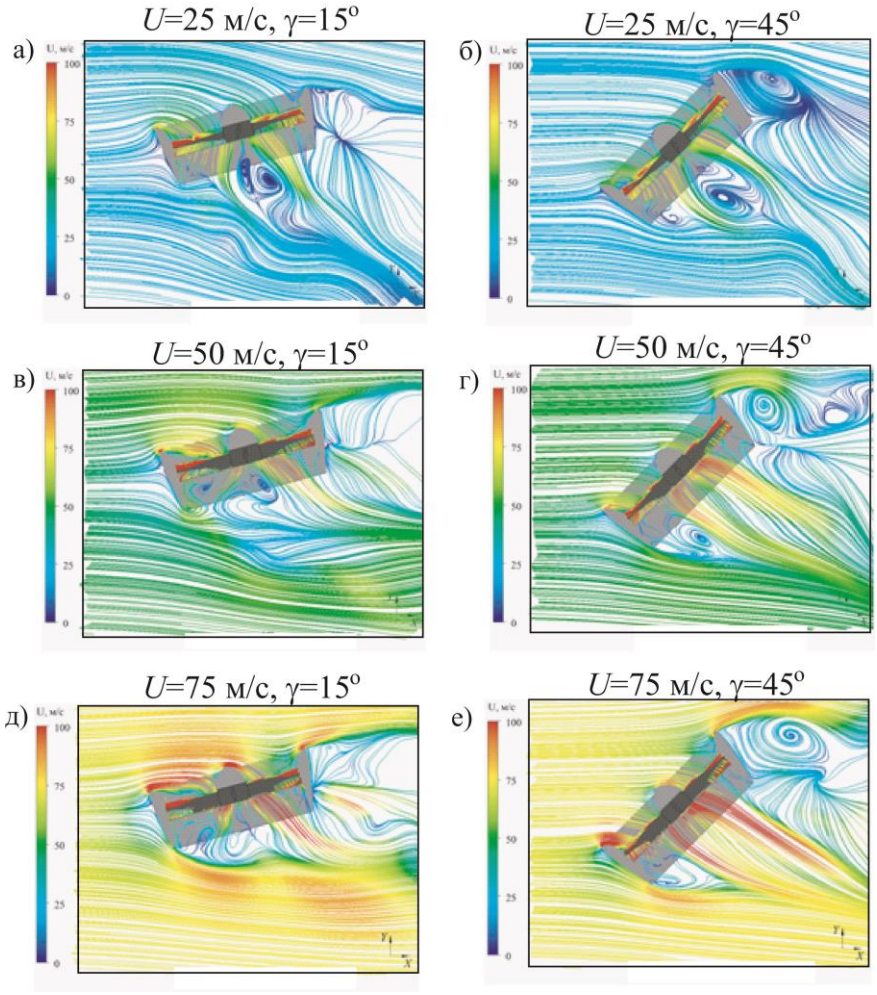

Figure 2. Influence of velocity in the outlet section of the ring and the angle of deflection from the vertical on the streamline pattern

A suction zone is observed in front of the rotor and to the side of it, the flow rate in which increases with approaching the rotor disk. The flow intensity decreases with approaching the rotor rotation axis, where low-speed turbulent structures are observed near the butt parts of the blades. Behind the propeller, the flow velocity reaches its maximum in the cone below the tip regions of the blades and decreases with further distance downstream of the propeller disk. The most intense turbulent

structures are end vortices descending from the tips of the blades and twisting into characteristic tapering spirals descending downstream from the plane of rotation of the rotor. With the distance from the propeller disk downstream, the intensity of turbulent structures decreases.

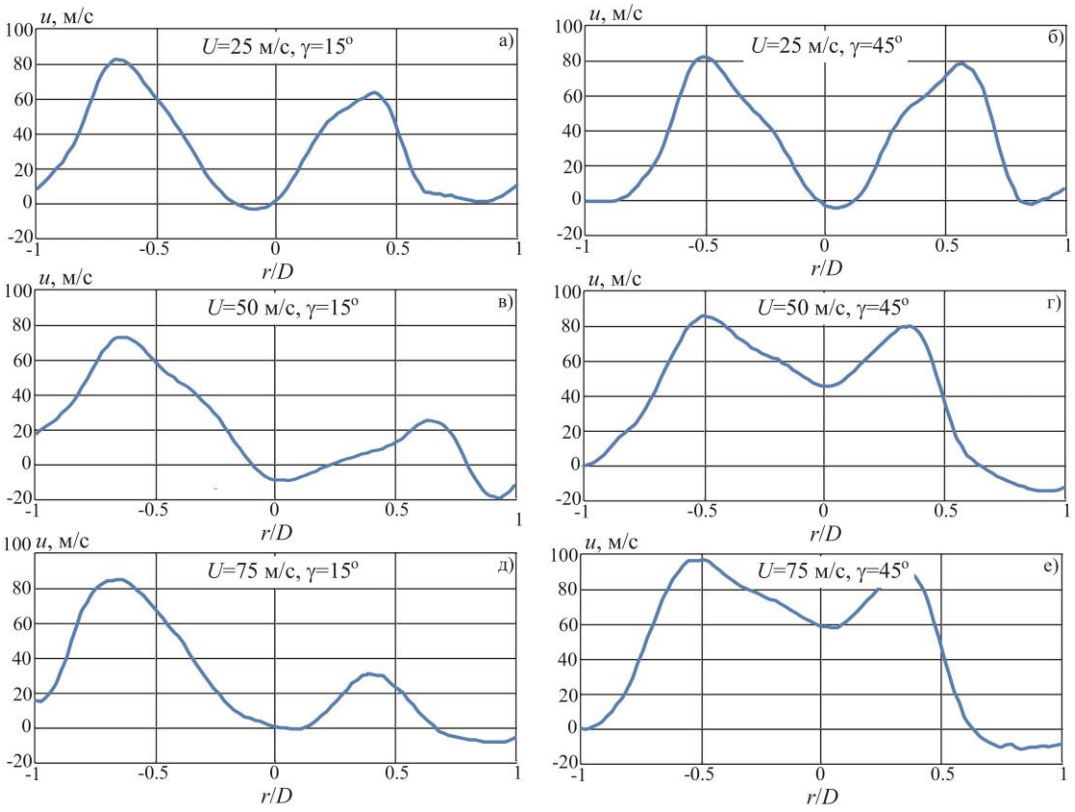

Figure 3. Influence of velocity in the outlet section of the ring and the angle of deflection from the vertical on the distribution of axial velocity

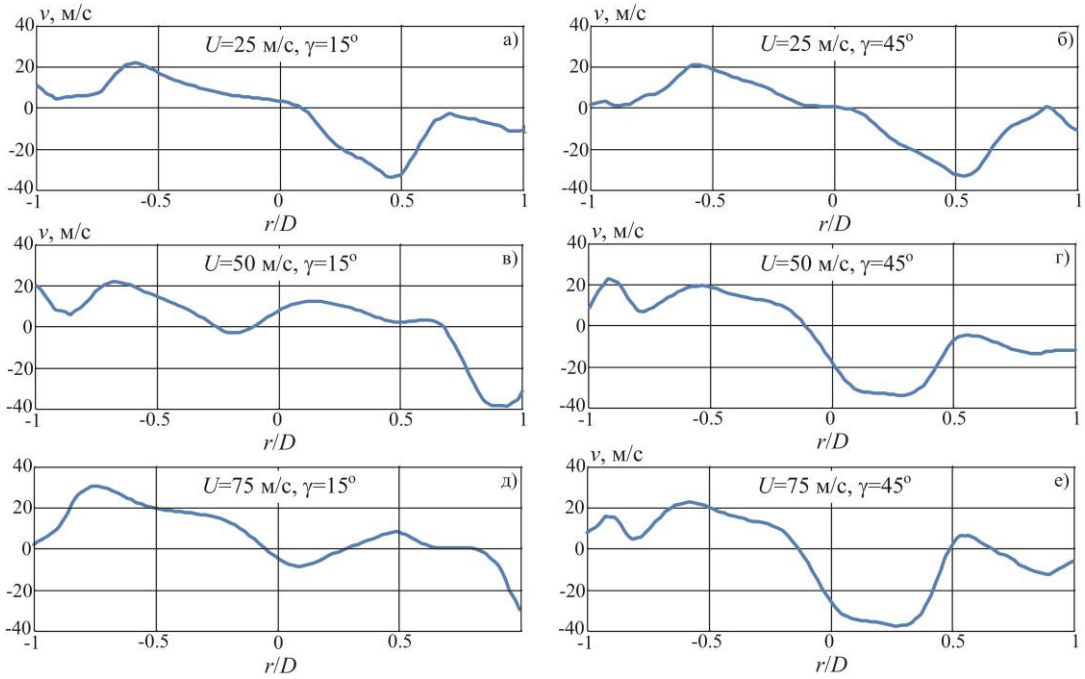

Figure 4. Influence of speed in the outlet section of the ring and the angle of deflection from the vertical on the distribution of peripheral speed

The distributions of the circumferential and axial velocity components in the outlet section of the ring at different incoming flow velocities and the impeller deviation angle from the vertical are shown in Fig. 3 and fig. 4.

The influence of the speed and angle of deviation of impeller from the vertical on the thrust characteristics is shown in Fig. 5.

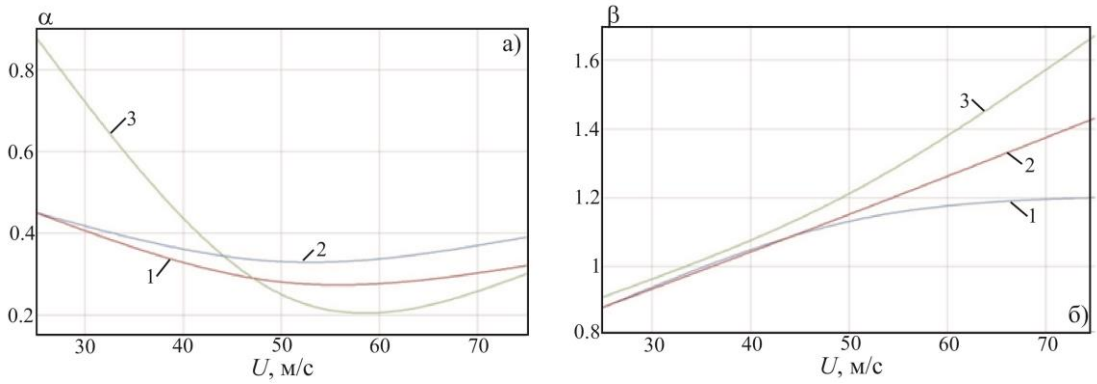

Figure 5. Dependence of the thrust factor (a) and power factor (b) on the oncoming flow velocity for various angles of deviation from the vertical γ=15° (1), 30° (2), 45°(3)

The results obtained show both the change in the total coefficient of the thrust force and the change in its constituent components (the thrust force of the propeller and the thrust force of the ring) depending on the speed of the incoming flow and the angles of deviation of the impeller from the vertical. The forces acting on the impeller and its elements for various incoming flow velocities and angles of impeller deviation from the vertical are shown in Fig. 6. The relative coefficient of the propeller thrust is a small value of the total thrust of the system. The high bearing capacity of the body is associated with the optimal configuration of the ring, which has a relatively large radius of the collector rounding and a sufficiently long diffuser [6]. High velocity at the duct wall increases manifold thrust.

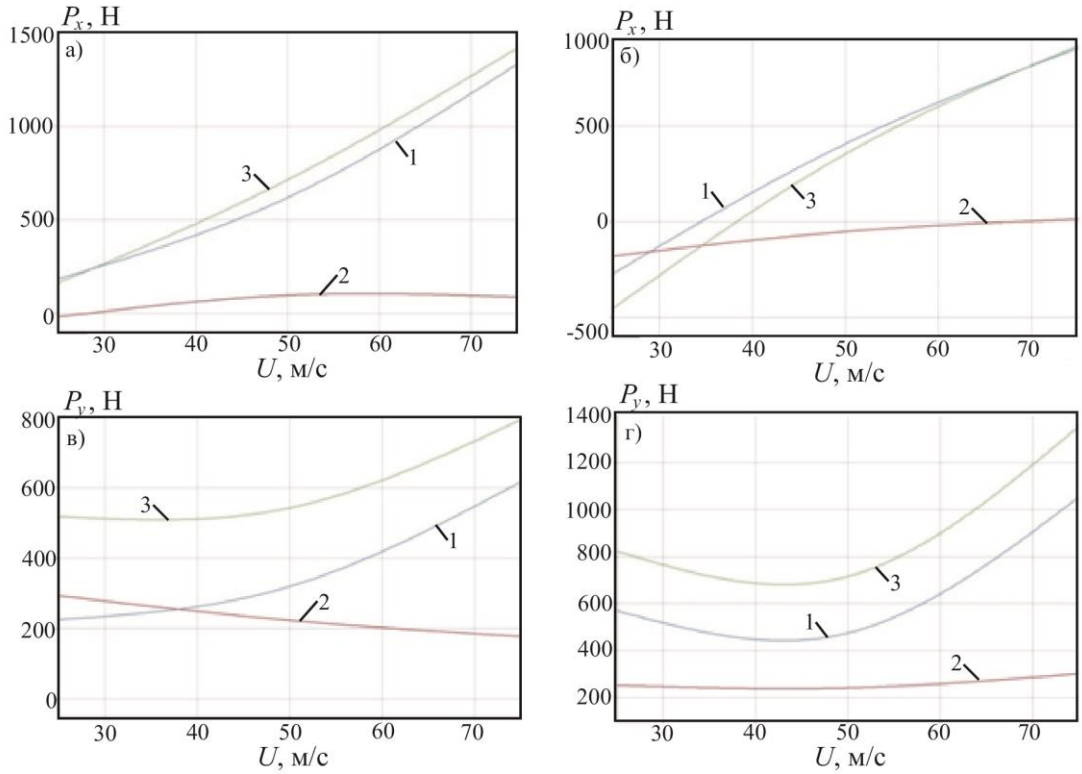

Figure 6. Dependences of the thrust projections on the x and y axes on the incoming flow velocity at γ = 15 ° (a, c), 45 ° (b, d) for the ring (1), propeller (2), ring and propeller (3)

The total system thrust coefficient and the propeller thrust coefficient at a zero angle of attack grow with increasing speed due to an increase in the mass air flow passing through the propeller. When the angle of deviation of impeller from the vertical is changed, the total thrust of the system is significantly reduced due to the drop in the thrust of the ring.

Summary

Modern approaches to modeling stationary and unsteady viscous incompressible fluid flows, in particular, the SST model and eddy-resolving approaches to turbulence modeling, are one of the UAV design tools. Numerical modeling allows not only to reduce the cost of setting up a physical experiment, but also supplements experimental research with new information necessary to find rational solutions at the development stage. At the tips of the propeller blades, vortex bundles are formed, the unsteady interaction of which with the underlying surface is important when considering the landing mode of the quadrocopter.

Problem-oriented means of numerical simulation of aerodynamic characteristics of impeller in various operating modes have been created.

Acknowledgement

This work was financially supported by the Ministry of Science and Higher Education of the Russian Federation during the implementation of the project "Fundamental Foundations of Mechanics, Monitoring and Control Systems for Unmanned Aviation Systems with Shaping Structures Deeply Integrated with Power Plants, and Unique Properties Not Used Today in Manned Aviation" FEFM-2020-0001.

References

1. Ostroukhov S.P. Aerodynamics of propellers and impellers // M.: FIZMATLIT - 2014, p. 328.
2. Buzykin O.G., Kazakov A.V., Shustov A.V. Numerical simulation of the aerodynamic characteristics of a small aircraft // TsAGI scientific notes. 2010. T. XLI. № 5. p. 21-31.
3. Nazarov D.V., Kondryakov A.V. Investigation of the propeller flow using numerical and experimental methods // Proceedings of the Russian Academy of Sciences, Samara Scientific Center. 2018. T. 20. № 4. p. 70-75.
4. Chovancova A., Fico T., Chovanec L., Hubinsky P. Mathematical modelling and parameter identification of quadrotor (a survey) // Procedia Engineering. 2014. Vol. 96. p. 172-181.
5. Golovkin M.A., Kochish S.I., Kritskiy B.S. Method for calculating the aerodynamic characteristics of the combined carrier system of the aircraft // Electronic journal «Trudy MAI». 2012. № 55. p. 1-16.
6. Moysikh E.I., Zavalov O.A., Kuznetcov A.V. Experimental studies of the aerodynamic characteristics of a remotely piloted aircraft with a ducted fan carrier system // Electronic journal «Trudy MAI». 2012 №. 50. p. 1-13.
7. Akturk A., Shavalikul A., Camci C. PIV measurements and computational study of a 5-inch ducted fan for V/STOL UAV applications // AIAA Paper. 2009. No. 2009-332.

8. Akturk A., Camci C. Experimental and computational assessment of a ducted-fan rotor flow model // Journal of Aircraft. 2012. Vol. 49. No. 3. P. 885-897.
9. Yilmaz S., Erdem D., Kavsaoglu M. Effects of duct shape on a ducted propeller performance // AIAA Paper. 2013. No. 2013-0803.
10. Akturk A., Camci C. Tip clearance investigation of a ducted fan used in VTOL unmanned aerial vehicles. Part I. Baseline experiments and computational validation // Journal of Turbomachinery. 2014. Vol. 136. No. 2. 021004 (10 pages).
11. Garipova L.I., Batrakov A.S., Kusymov A.N., Mikhaylov S.A., Barakos D. Determination of the aerodynamic characteristics of the main rotor model in the axial flow mode // Proceedings of higher educational institutions. Aviation technology. 2014. № 3. p. 7-13.
12. Biava M., Barakos G.N. Optimisation of ducted propellers for hybrid air vehicles using high-fidelity CFD // The Aeronaut Journal. 2016. Vol. 120. No. 1232. p. 16321657.
13. Chen J., Li L., Huang G., Xiang X. Numerical investigations of ducted fan aerodynamic performance with tip-jet // Aerospace Science and Technology. 2018. Vol. 78. p. 510-521.
14. Xu H.-Y., Xing S.-L., Ye Z.-Y. Numerical study of ducted-fan lip stall suppression based on inflatable leading lip cell // Procedia Engineering. 2015. Vol. 126. p. 158-162.
15. Ohanian O.J., Karni E.D., Londenberg W.K., Gelhausen P.A., Inman D.J. Ducted-fan force and moment control via steady and synthetic jets // Journal of Aircraft. 2011. Vol. 48. No. 2. p. 514-526.
16. Zhang T., Barakos G.N. Review on ducted fans for compound rotorcraft // The Aeronautical Journal. 2020. Vol. 124. No. 1277. p. 941-974.
17. Diizy F., Barakos D., Kusymov A.N., Kusymov S.A., Mikhaylov S.A., DES-modeling of the helicopter main rotor flow // Proceedings of higher educational institutions. Aviation technology. 2018. № 1. p. 40-46.

18. Rumsey C.L., Biedron R., Farassat F., Spence P. Ducted-fan engine acoustic predictions using a Navier-Stokes code // Journal of Sound and Vibration. 1998. Vol. 213. No. 4. p. 643-664.
19. Reboul G., Polacsek C., Lewy S., Heib S. Aeroacoustic computation of ducted-fan broadband noise using LES data // Journal of Acoustic Society of America. 2008. Vol. 123. No. 5. p. 3539-3539.
20. Rhee W., Myers L., Mclaughlin D. Aeroacoustics of vertical lift ducted rotors // AIAA Paper. 2009. No. 2009-3333.
21. Astley R., Sugimoto R., Achunche I., Kewin M., Mustafi P., Deane E. A review of CAA for fan duct propagation and radiation, with application to liner optimisation // Procedia Engineering. 2010. Vol. 6. p. 143-152.
22. Malgoezar A.M., Vieira A., Snellen M., Simons D.G., Veldhuis L.L. Experimental characterization of noise radiation from a ducted propeller of an unmanned aerial vehicle // International Journal of Aeroacoustics. 2019. doi:10.1177%2F1475472X19852952
23. Volkov K. Numerical analysis of Navier-Stokes equations on unstructured meshes // Handbook on Navier-Stokes Equations: Theory and Analysis / D. Campos. Nova Science, 2016. p. 365-442.
24. Volkov K. Multigrid and preconditioning techniques in CFD applications // CFD Techniques and Thermo-Mechanics Applications / Z. Driss, B. Necib, H.-C. Zhang. Springer International Publishing, 2018. p. 83-149.